RESEARCH ARTICLE | DECEMBER 28 2023

Isotropic exchange-bias in twinned epitaxial Co/Co_3O_4 bilayer

Martin Wortmann ; Tapas Samanta ; Maik Gaerner ; Michael Westphal; Johannes Fiedler; Inga Ennen; Andreas Hütten ; Tomasz Blachowicz ; Luana Caron; Andrea Ehrmann

APL Mater. 11, 121118 (2023)
https://doi.org/10.1063/5.0183566

Isotropic exchange-bias in twinned epitaxial Co/Co_3O_4 bilayer

Cite as: APL Mater. 11, 121118 (2023); doi: 10.1063/5.0183566
Submitted: 23 October 2023 • Accepted: 6 December 2023 •
Published Online: 28 December 2023

Martin Wortmann,[1,a)] Tapas Samanta,[1] Maik Gaerner,[1] Michael Westphal,[1] Johannes Fiedler,[2] Inga Ennen,[1] Andreas Hütten,[1] Tomasz Blachowicz,[3] Luana Caron,[1,4] and Andrea Ehrmann[2]

AFFILIATIONS

[1] Bielefeld University, Faculty of Physics, Universitätsstraße 25, 33615 Bielefeld, Germany
[2] Bielefeld University of Applied Sciences and Arts, Faculty of Engineering and Mathematics, Interaktion 1, 33619 Bielefeld, Germany
[3] Silesian University of Technology, Institute of Physics—Center for Science and Education, 44-100 Gliwice, Poland
[4] Helmholtz-Zentrum Berlin für Materialien und Energie, Berlin 12489, Germany

[a)] **Author to whom correspondence should be addressed:** mwortmann@physik.uni-bielefeld.de

ABSTRACT

Exchange bias (EB) is a unidirectional anisotropy caused by interface coupling between a ferromagnet and an antiferromagnet. It causes a preferential direction of magnetization in the ferromagnet, which manifests as a shift of the hysteresis loop along the magnetic field axis. Here, we demonstrate a large EB of over 1000 Oe at 20 K in a twinned Co(111)/Co_3O_4(111) thin film epitaxially grown on sapphire(0001) with sixfold rotational lattice symmetry, which is among the highest values reported for Co/$Co_{1-y}O$ systems. In such systems, the effect intensity is largest along the magnetic easy axes, which usually results in an anisotropy of the EB in epitaxial interfaces. However, we observed identical EB values for 0°, 15°, and 30° angles between the magnetic field and the nearest Co[002] magnetic easy axes. The measurements imply a relaxation of the magnetization to the nearest easy axis, suggesting increasingly isotropic EB fields with higher orders of rotational lattice symmetry.

I. INTRODUCTION

After being discovered in 1956,[1] the exchange bias (EB) phenomenon was intensively investigated in experiment and theory for spintronic applications.[2] The most common EB system consists of a ferromagnet (FM) exchange-coupled to an antiferromagnet (AFM), which causes a horizontal shift of the hysteresis loop H_{EB} after field cooling (FC) through the Néel temperature T_N. This effect is often accompanied by a vertical loop shift and an asymmetry of the hysteresis loop.[3,4]

The EB was first discovered in Co/CoO, which is still among the most frequently investigated oxide-based EB model systems.[5,6] Besides core-shell nanoparticles[7,8] and nanostructures,[2,9] Co/CoO is often examined in the form of thin-film systems. Co/Co_3O_4 is another typical model system for a ferromagnet combined with a diluted antiferromagnet, as described in the domain state model.[10,11] Co/Co-oxide thin-film systems can be grown in different orientations depending on the crystal orientation of the substrate, which results in different anisotropies and EB fields.[5] The EB is also known to depend on the AFM and FM layer thickness.[9,12,13]

Generally, Co/CoO and Co/Co_3O_4 thin film structures can exhibit EB fields in a broad range. Beschoten *et al.* found values ranging from ~200 to 800 Oe after FC to 20 K depending on the thickness and oxygen dilution of the $Co_{1-y}O$ layer.[11] Krivorotov *et al.* reported a similar value around 650 Oe for macroporous Co/CoO film systems.[14] Smaller EB shifts of 60–180 Oe at 20 K were reported by Kumar *et al.* for polycrystalline Co/CoO bilayers with different interface roughness,[15] while the AFM grain size was shown to increase the EB field from about 100 Oe to 200 Oe.[16] Larger EB shifts than the ones mentioned are usually not found in Co/CoO or Co/Co_3O_4 thin film systems. Most recently, Co/Co_3O_4 nanorod arrays have been found to show a relatively small EB of 35–60 Oe,[17] while Co/CoO core shell nanostructures exhibited much larger EB values of up to ~600 Oe at low temperatures.[18,19]

The blocking temperatures of the antiferromagnets CoO and Co_3O_4, above which no EB occurs, are significantly different, corresponding to Néel temperatures of $T_N \approx 295$ K (CoO) and $T_N \approx 40$ K (Co_3O_4), respectively, leading to vastly different temperature dependencies of such systems.[20] Nevertheless, some studies on Co/Co_3O_4 bilayer systems already showed that an EB can occur up to a temperature of 220 K[21] or even higher.[22] Systems with overoxidized $Co_{1-y}O$, where large EB shifts were found even near room temperature,[10,11] make it clear that it is important to investigate the precise crystal structure and composition of the AFM. (111)-oriented Co/$Co_{1-y}O$ systems with their threefold crystallographic symmetry are expected to show less pronounced magnetic anisotropy compared to (110)-oriented systems with only twofold symmetry[5] due to smaller angles to the nearest magnetic easy axis in the (111)-orientation.

Here, we report on the synthesis, detailed structural characterization, and magnetization measurements of a twinned Co(111)/Co_3O_4(111) bilayer system with sixfold crystallographic symmetry on an Al_2O_3(0001) (sapphire) substrate. Temperature- and angle-dependent magnetization measurements reveal a large isotropic EB field of more than 1000 Oe at 20 K, which is among the highest values reported for Co/$Co_{1-y}O$ systems. While several studies have been published about different aspects of Co/Co_3O_4 EB systems, most of them only investigate one specific field-to-sample orientation. Nearly isotropic EB and coercive fields were, to the best of our knowledge, not yet reported for highly crystalline and thus anisotropic Co/Co_3O_4 EB systems. In addition, the EB described in this work is very large, making the system highly relevant for technical applications.

II. EXPERIMENTAL

The sample was grown epitaxially by molecular beam epitaxy (MBE) on an Al_2O_3(0001) substrate (dimensions 10×5 mm^2; space group: $Fm\bar{3}m$) in the stacking order Al_2O_3/Co/Co_3O_4. The Co_3O_4 layer was grown at an oxygen partial pressure of $p(O_2) = 5 \times 10^{-6}$ mbar in the UHV MBE chamber, resulting in over-oxidation as compared to pure CoO. For comparison, Beschoten *et al.* found that a partial oxygen pressure of $p(O_2) = 3.3 \times 10^{-7}$ mbar during growth by MBE results in an unintentionally diluted CoO layer, while $p(O_2) = 5 \times 10^{-6}$ mbar led to optimal dilution regarding the EB shift.[11]

X-ray diffractometry (XRD) and x-ray reflectometry (XRR) measurements were performed with a X'Pert Pro MPD PW3040-60 diffractometer (PANalytical) using Cu Kα radiation ($\lambda = 1.540\,56$ Å).

The surface chemistry of the samples was examined by x-ray photoelectron spectroscopy (XPS) in an Omicron Multiprobe Ultra-High Vacuum system (Scienta Omicron) at 7×10^{-11} mbar using monochromatic Al Kα irradiation. The electron emission angle was 77° and the source to analyzer angle was 54.7°. The core-level spectra were recorded with an acquisition time of 0.8 s per 0.05 eV with a pass energy of 15 eV in a constant analyzer energy mode. The sample was grounded via a small piece of conductive carbon tape. The Fermi level cutoff was observed at −0.28 eV binding energy, and no referencing was performed. The spectrum contained a relatively strong carbon signal originating from adventitious carbon. No sputter etching was performed to clean the sample from adventitious carbon as Co_3O_4 can be reduced to CoO by ion bombardment.[23] The CasaXPS software (version 2.3.22PR1.0) was used for peak deconvolution. All Co 2p components were fitted on an E Tougaard background with symmetric Voigt line shapes GL(30) except for the metallic Co components, which were fitted using Lorentzian asymmetric line shapes LA(1,5,200). All spin–orbit-split peak pairs, including the satellite features, were constrained by the known ratio of 1:2 for p-orbitals. The Co^{2+} to Co^{3+} ratio was set to 1:2 according to the expected $Co^{2+}(Co^{3+})_2(O^{2-})_4$ structure. The O 1 s components were fitted with GL(40) line shapes. The component ascribed to adsorbed species is broader than the others as C bonded O of adventitious carbon is known to be broadly distributed between 530 and 534 eV.

The microstructure of the sample has been investigated by transmission electron microscopy (TEM) employing a JEM 2200FS (JEOL) operated at 200 kV. The TEM is equipped with an omega filter for electron energy loss spectrometry (EELS) and an energy dispersive x-ray spectrometer (EDX) for elemental mappings. The cross-sectional lamella has been prepared using a FEI Helios dual beam FIB operated at 30 kV beam energy with a subsequent ion polishing step at 5 kV.

The in-plane (IP) and out-of-plane (OOP) magnetization measurements of the thin film sample were performed using the VSM mode of a MPMS 3 magnetometer (Quantum Design). The sample was cooled down from 350 K in the presence of 1 T magnetic field before starting the isothermal field loop measurements $M(\mu_0 H)$ for each temperature.

III. RESULTS AND DISCUSSION

A. Crystal structure

The film growth during MBE was monitored by *in situ* reflection high-energy electron diffraction (RHEED) (patterns shown in Fig. S1 of the supplementary material). Its crystal structure was determined by XRD. Both RHEED and the specular $\theta - 2\theta$ XRD scan confirm that Co (space group: $Fm\bar{3}m$) and Co_3O_4 (space group: $Fd\bar{3}m$) grow in the fcc(111) orientation consisting of two sublattices with 60° azimuthal difference. This structural domain twinning results from two incompatible stacking orders, ABC and ACB, as illustrated in Fig. 1(a). The degree of twinning in Co and Co_3O_4 was estimated using off-specular XRD texture mapping. The mappings were carried out for an IP sample rotation of $\Phi = 360°$ and an OOP sample tilt of $\Psi = \langle 50°, 60° \rangle$. The coordinate system, as shown in Figs. 1(c) and 1(d), is chosen in such a way that the sapphire $\{10\bar{1}2\}$ peak is located at $\Phi = 0°$ upon a sample tilt of $\Psi = 57.60°$.

The diffraction peaks of Co{002} at $2\theta = 51.37°$ and $\Psi = 54.7°$ (green and blue for the different phases) and of Co_3O_4{004} at $2\theta = 44.82°$ and $\Psi = 54.7°$ (light and dark purple) are shown in Figs. 1(c) and 1(d), respectively. The diffraction peaks of both layers are located at the same Φ-positions, indicating that the Co and Co_3O_4 layers share the same crystallographic orientation with respect to the substrate. Also shown in Fig. 1(c) are three sapphire $\{20\bar{2}4\}$ peaks (red), which occur at $\Psi = 57.6°$.

Figure 1(e) shows $\theta - 2\theta$ scans of the Co_3O_4(004) and Co(002) diffraction peaks of the twinned phases A and B at $\Phi = 30°$ and $\Phi = 90°$, respectively. The amount of twinning can be determined using the ratio of the integrated peak intensities corresponding to

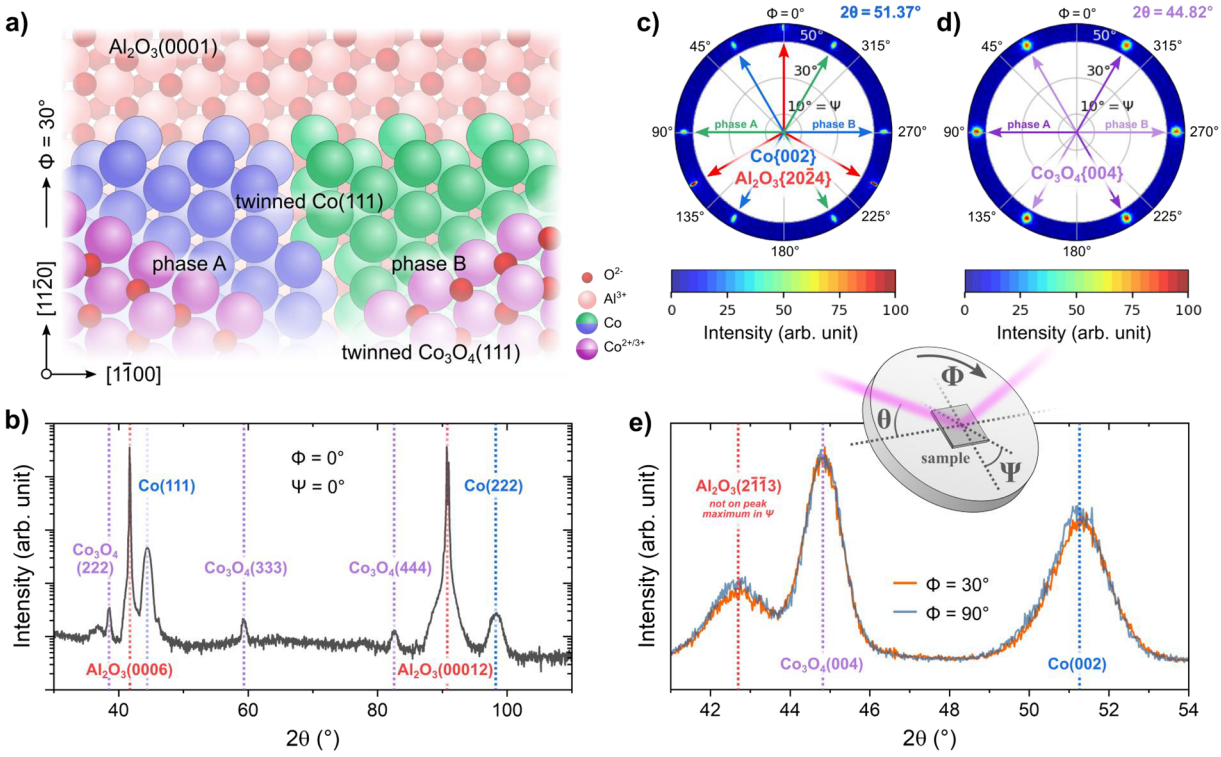

FIG. 1. Crystal structure: (a) Schematic illustration of the crystal structures of the sapphire(0001) substrate, the Co(111) FM layer, and the Co_3O_4(111) AFM layer. (b) Specular $\theta - 2\theta$ XRD scan. (c) XRD texture maps showing the twinned threefold symmetry of the FM (blue/green arrows) and (d) AFM (light/dark purple arrows) layers with respect to the substrate orientation (red arrows). (e) Specular $\theta - 2\theta$ XRD scan at $\Phi = 30°$ and 90°, both at $\Psi = 54.7°$. The inset shows a schematic illustration of the measurement setup.

phases A and B. For the Co_3O_4 and Co layers, the amounts of twinning are estimated to be 100% (i.e., 50% phase A and 50% phase B) and 99% (i.e., 51% phase A and 49% phase B), respectively, within a margin of error of 2%. Both layers can therefore be regarded as fully twinned.

B. Morphology and composition

The XPS measurements, as shown in Fig. 2(a), are in good agreement with the expected Co_3O_4 structure. Beneath a layer of atmospheric carbon and an outer $Co^{2+}(OH^-)_2$ hydroxide layer, the lattice O^{2-} to $Co^{2+/3+}$ atomic ratio resulting from the fit model is 0.73, just below the nominal value of 0.75. The spectrum suggests the presence of trace metallic Co (about 2.5% of the total Co signal), which is unlikely to originate from the underlying metallic Co layer as the oxide layer is too thick. The O^{2-} to total Co atomic ratio resulting from the fit model is 0.75. Although these results somewhat depend on fit constraints and background type, the measurement confirms the Co_3O_4 stoichiometry within a reasonable margin of error.

Figure 2(b) shows XRR data with the layer thicknesses d, densities ρ, and roughnesses σ obtained as fit parameters. A satisfactory fit could only be achieved considering an additional top-layer of hydroxide and adventitious carbon as revealed by XPS. The resulting thicknesses are $d = 7.5$ nm and $d = 22.2$ nm for Co and Co_3O_4, respectively. The interface roughnesses steadily increase from the substrate to the top-layer (fit parameters of the top-layer: $d = 0.5$ nm, $\sigma = 3.0$ nm). The rather low density of the Co layer may indicate lattice defects at the grain boundaries as implied by the TEM images.

The TEM images in Fig. 2(c) show the sample cross section with multiple grain boundaries. The images are in good agreement with the XRR and XRD measurements. The corresponding electron energy loss spectrum (EELS) in Fig. 2(d) shows the characteristic Co L_3 and Co L_2 ionization edges. In the spectrum measured in the Co layer (EELS_1), the peaks occur at 782 and 798 eV. In the spectrum measured in the Co_3O_4 layer (EELS_2), the peaks are shifted by about 1.5 eV toward higher energy. The EDX mapping in Fig. 2(d) reveals that the boundaries between Co grains are oxidized down to the substrate. The comparatively lower oxygen concentration between the Co grains indicates but cannot with certainty be attributed to oxygen deficiency of Co_3O_4 (possibly in the form of CoO) as the grain boundaries may overlap with Co grains perpendicular to the plane of the TEM lamella.

Figure 2(e) shows representative SEM images of the sample surface. The structural domains (light regions) are about 50–100 nm in lateral dimensions. They are clearly distinguishable by randomly oriented grain boundaries (dark regions).

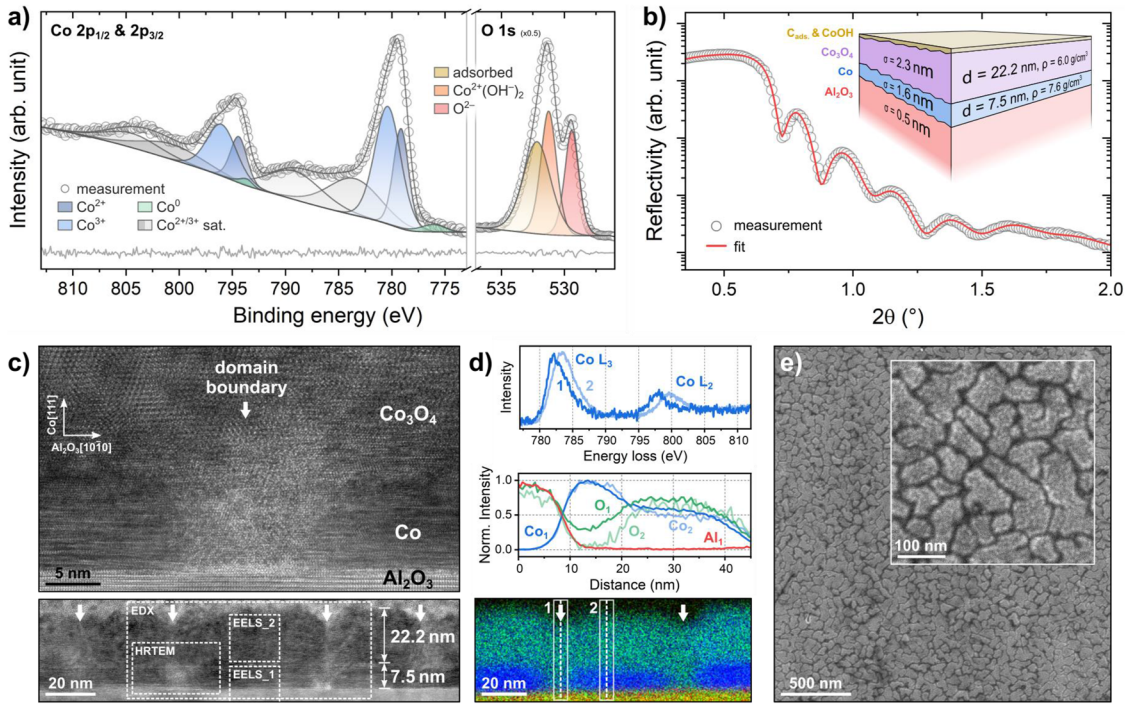

FIG. 2. Chemical and morphological characterization: (a) XPS Co 2p and O 1s core-level spectra of Co_3O_4. Fit residuals are shown in gray below the data. (b) XRR measurement with a schematic illustration of the thickness d, density ρ, and roughness σ resulting from the fit. (c) HRTEM images of the sample cross section. White arrows indicate grain boundaries. (d) EELS spectra (top) of Co (blue) and Co_3O_4 (light blue) and EDX line profiles (middle). The indices in the diagrams refer to the white boxes in the TEM image and EDX mapping (bottom). Elements are colored in red = Al, green = O, and blue = Co. (e) SEM images of the sample surface (average lateral grain area is ~5000 nm^2).

C. Magnetic properties

Figures 3(a)–3(c) show magnetic hysteresis loops measured at an angle between the external magnetic field and the [10$\bar{1}$0] orientation of the Al_2O_3 substrate of 0°, 45°, and 90°, corresponding to 0°, 15°, and 30° with respect to the nearest Co[002] magnetic easy axis in one of the twinned lattices; OOP magnetization curves are shown in Fig. 1(d). Generally, all IP measurements showed similar sets of hysteresis loops for the investigated temperatures between 10 and 300 K.

A small dent in the magnetization reversal from positive to negative saturation after crossing zero magnetic field (indicated by green arrows) is clearly visible at the 15° field-to-easy axis orientation in Fig. 3(b), less so at 0° in Fig. 3(a), and not at all at 30° in Fig. 3(c). Such an asymmetry is often recognized in EB systems and commonly attributed to different magnetization reversal processes on either side of the hysteresis curve.[24] In thin-film systems, it might be caused by the relaxation of the magnetization toward the nearest easy axis near the zero external magnetic field. This effect is especially well known from systems such as Fe/MnF_2 where the FM magnetization relaxes toward the nearest easy axis at vanishing external magnetic field.[25] However, in Co/$Co_{y-1}O$ systems, it is usually less pronounced than in systems with strong magnetic anisotropy of the AFM.[25] Here, the dent is correspondingly strongest for a field-to-sample orientation of 45°, as seen in Fig. 3(b), i.e., only 15° to the nearest easy axis, so that relaxation can easily occur at remanence. This becomes visible as rotation of the magnetization away from the measurement axis and thus as a dent. On the other hand, no such dent is visible for the 90° field-to-sample orientation, where the external magnetic field is oriented parallel to an easy axis, as seen in Fig. 3(c), so that no rotation of the magnetization occurs at remanence.

Although the saturation magnetization is consistent for all IP measurements, it is smaller by three orders of magnitude in the OOP magnetization curves. It is well known that only a small OOP component of magnetization can be expected in Co/CoO(111) systems because the AFM moments are oriented at 8° OOP.[26] Typically, OOP magnetization in Co/CoO or Co/Co_3O_4 EB systems can be triggered by a nanostructure of the sample[27,28] by using Co/Pt[29] or Co/CoO multilayers,[30] but it has also been reported for oxygen ion implantation in Co thin films where a strong OOP magnetization of the top surface was found, while the magnetization in the lower layers was oriented IP.[31] For the case of such buried uncompensated spins, a micromagnetic simulation by Menéndez *et al.* attributed the training effect (i.e., the reduction of the EB for subsequent hysteresis loops) and asymmetric magnetization reversal to the perpendicular anisotropy.[32]

Only a few investigations of the OOP EB in Co/Co_{0031-y}Co thin-film systems can be found in the literature. Wu *et al.* prepared

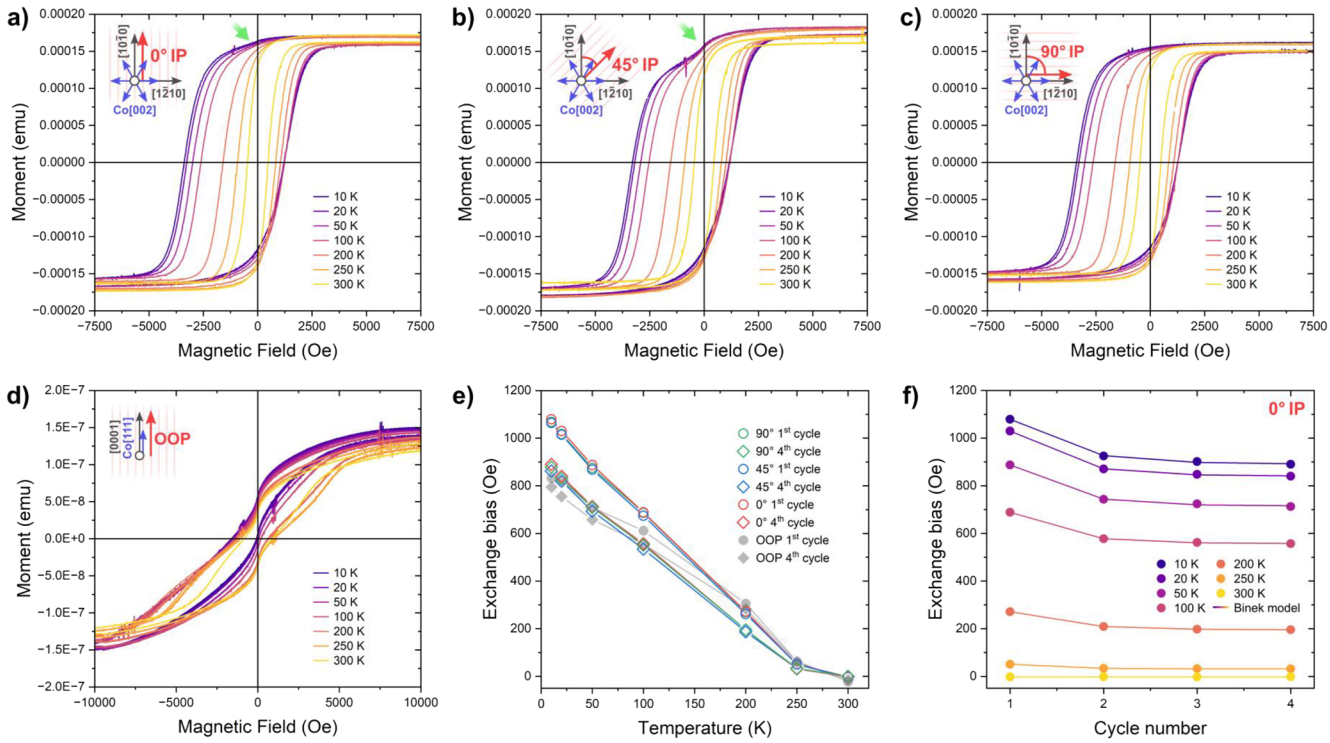

FIG. 3. Magnetic properties: magnetic hysteresis curves during the first field cycle at different temperatures with the applied magnetic field in field-to-sample orientations of (a) 0°, (b) 45°, and (c) 90° IP and (d) OOP. The schematics show the field orientation relative to the crystal lattice. Note that Co[002] has an OOP component, which is not shown here. All data have been linearized at saturation by convolution with an arbitrary linear function to account for the diamagnetic substrate contribution. (e) EB over temperature for the aforementioned field-to-sample orientations during first and last (forth) field cycle. (f) EB over field cycle number showing the training effect. The shown data are only from the 0° IP orientation as all IP orientations are essentially congruent (45° and 90° IP orientations are shown in Fig. S2 of the supplementary material).

granular Co films with a naturally oxidized CoO layer on top and reported much smaller EB and coercive fields than those in the IP orientation, as well as a positive EB for a 3.6 nm thick film, of which ~2 nm were oxidized.[33] The FM and AFM layers in our study were much thicker and epitaxially grown; therefore, such effects were not observed. Ovejero *et al.* investigated thick magnetron-sputtered Co/CoO layers and found larger coercive fields in OOP than in IP magnetization measurements.[34] Similar to our results, they reported a two-step magnetization reversal for OOP magnetization measurements. This finding was attributed to a preferential EB direction for an intermediate cooling field, as no two-step process was observed when the AFM surface was fully oriented at higher cooling fields. Comparing these samples with either much higher or much lower layer thicknesses than in this study, we found smaller coercive fields and a two-step magnetization reversal process in OOP measurements, combining effects of both aforementioned studies.

Unexpectedly, the EB, as depicted in Fig. 3(e), is virtually identical in all IP field orientations and very similar to the OOP hysteresis loops. The EB values are also larger compared to those previously reported in the literature for similar samples and temperatures.[11,14–16] The blocking temperature is ~260 K, i.e., slightly below T_N of CoO (293 K), but significantly higher than T_N of Co_3O_4 (~40 K). The occurrence of an EB above T_N of Co_3O_4 in Co/Co_3O_4 samples has been reported in the literature and is usually attributed to the presence of CoO at the FM–AFM interface.[21,22] If that is the case, its amount is insufficient to be detected by XRD. However, the apparent disorder and oxygen deficiency at the grain boundaries, as revealed by TEM measurements, may indeed suggest the presence of CoO.

The coercivity (see Fig. S3 in the supplementary material) is very similar for all IP measurements. From Brillouin light scattering measurements of Co(111)/CoO(111) samples at different temperatures, it is well-known that a weak sixfold magnetic anisotropy occurs below and above the blocking temperature.[5] While epitaxial Co/CoO and Co/Co_3O_4 grown on MgO(110) substrates with twofold anisotropy was reported to result in angle-dependent EB and coercivity,[5] no such reports were found for the angle-dependence in Co(111)/CoO(111) or $Co(111)/Co_3O_4(111)$.

In this study, FC was performed in an intermediate cooling field. Taking into account the suggestion of Ovejero *et al.*[34] that intermediate cooling fields only partially align the AFM domains, it could be speculated that in the case of epitaxially grown films with more than two energy minima, i.e., higher than twofold structural anisotropy, the orientation of the AFM domains is distributed in orientations parallel to the easy axis, which are nearest to the cooling field direction. In other words, FC along 90°, which is an easy axis,

would result in all AFM domains being oriented in the 90° direction, resulting in the EB being oriented in the 90° direction. FC along 0°, on the other hand, would result in the AFM domains being oriented along −30° or +30°, i.e., along the easy axes nearest to the cooling field direction. This would result in the EB being oriented in the 0° direction, as expected, with a similar value as for FC along 90°. In EB systems with twofold symmetry, on the other hand, FC along the hard axis should result in a much weaker EB compared to FC along the easy axis, as it was, indeed, previously reported.[5]

The random distribution of grain boundaries and correspondingly of magnetic domain wall orientations, as seen in the SEM images in Fig. 2(e), could further contribute to the isotropy of the EB. While such a fractal domain structure was also found for AFMs with different properties in Monte Carlo simulations, serving as the theoretical basis for the domain state model,[35] it was not yet used to calculate the impact on the angle-dependence of the EB.

Finally, Fig. 3(f) shows the training effect for the first four hysteresis loops measured after FC to the respective temperatures. The training effect is often attributed to rotatable uncompensated interface spins.[36–38] For Co/CoO systems, other explanations include the formation of a stable AFM multidomain state after the first hysteresis measurement,[39] generally irreversible changes of the AFM domain upon measurements,[40] or even a change of the reversal mechanism in the descending branch after the first loop.[41,42] The latter was shown to depend on the creation of interfacial domains during the first reversal.[42] Especially at lower temperatures, a strong reduction of the EB from the first to the second field cycle was observed, which was often interpreted as an athermal effect.[13,43,44] Binek *et al.* showed that this behavior can be better modeled by their equation based on the discretized Landau–Khalatnikov equation than by a power law and can be attributed to the spin configurational relaxation at the interface.[45,46] This model was fitted to the training effect data, as shown by the straight lines in Fig. 3(f).

IV. CONCLUSION

We examined the field-direction-dependent exchange bias in a twinned epitaxial Co(111)/Co_3O_4(111) bilayer system grown on a sapphire(0001) substrate using molecular beam epitaxy. The measured EB of over 1000 Oe is among the highest values reported for Co/$Co_{1-y}O$ systems. Unexpectedly, field cooling along a hard, an easy, and an intermediate axis resulted in virtually isotropic EB fields below the blocking temperature of ~260 K. We attribute this unexpected isotropy to a splitting of the exchange bias direction into the Co[002] easy axes nearest to the cooling field direction when field cooling is performed along a hard axis.

SUPPLEMENTARY MATERIAL

The supplementary material contains the following: 1. RHEED images measured *in situ* during MBE-deposition, 2. training effect data for 45° and 90° sample-to-field orientations, and 3. coercivity over temperature.

ACKNOWLEDGMENTS

The authors acknowledge the support for the publication costs by the Open Access Publication Fund of Bielefeld University and the Deutsche Forschungsgemeinschaft (DFG). This work was carried out in the framework of the Joint Lab BiBer. The authors would like to thank Prof. Dr. Armin Gölzhäuser and Prof. Dr. Günter Reiss from Bielefeld University for providing access to their laboratories. Furthermore, the authors would like to thank Dr. Karsten Rott and Laila Bondzio for the sample preparation for TEM.

AUTHOR DECLARATIONS

Conflict of Interest

The authors have no conflicts to disclose.

Author Contributions

Martin Wortmann: Conceptualization (equal); Formal analysis (equal); Investigation (equal); Visualization (lead); Writing – original draft (lead); Writing – review & editing (lead). **Tapas Samanta**: Formal analysis (equal); Investigation (equal). **Maik Gaerner**: Formal analysis (equal); Investigation (equal). **Michael Westphal**: Investigation (equal). **Johannes Fiedler**: Formal analysis (equal); Software (equal). **Inga Ennen**: Investigation (equal). **Andreas Hütten**: Funding acquisition (equal); Resources (equal); Supervision (equal); Writing – review & editing (equal). **Tomasz Blachowicz**: Formal analysis (equal); Writing – review & editing (equal). **Luana Caron**: Funding acquisition (equal); Resources (equal); Supervision (equal); Writing – review & editing (equal). **Andrea Ehrmann**: Conceptualization (equal); Formal analysis (equal); Investigation (equal); Software (equal); Writing – original draft (equal); Writing – review & editing (equal).

DATA AVAILABILITY

The data that support the findings of this study are available from the corresponding author upon reasonable request.

REFERENCES

[1] W. H. Meiklejohn and C. P. Bean, "New magnetic anisotropy," Phys. Rev. **102**, 1413–1414 (1956).
[2] R. Morales, A. N. Flores, N. M. Vargas, J. Giuliani, I. K. Schuller, and C. Monton, "Ultradense arrays of sub-100 nm Co/CoO nanodisks for spintronics applications," ACS Appl. Nano Mater. **3**(5), 4037–4044 (2020).
[3] J. Nogués, T. J. Moran, D. Lederman, I. K. Schuller, and K. V. Rao, "Role of interfacial structure on exchange-biased FeF_2–Fe," Phys. Rev. B **59**, 6984–6993 (1999).
[4] T. Blachowicz, A. Ehrmann, and M. Wortmann, "Exchange bias in nanostructures: An update," Nanomaterials **13**(17), 2418 (2023).
[5] T. Blachowicz, A. Tillmanns, M. Fraune, R. Ghadimi, B. Beschoten, and G. Güntherodt, "Exchange-bias in (110)-oriented CoO/Co bilayers with different magnetocrystalline anisotropies," Phys. Rev. B **75**, 054425 (2007).
[6] V. Schneider, A. Reinholdt, U. Kreibig, T. Weirich, G. Güntherodt, B. Beschoten, A. Tillmanns, H. Krenn, K. Rumpf, and P. Granitzer, "Structural and magnetic properties of Ni/NiOxide- and Co/CoOxide core/shell nanoparticles and their possible use for ferrofluids," Z. Phys. Chem. **220**, 173–187 (2006).
[7] J. A. González, J. P. Andrés, R. López Antón, J. A. de Toro, P. S. Normile, P. Muniz, J. M. Riveiro, and J. Nogués, "Maximizing exchange bias in Co/CoO core/shell nanoparticles by lattice matching between the shell and the embedding matrix," Chem. Mater. **29**, 5200–5206 (2017).
[8] G. Salazar-Alvarez, J. Geshev, S. Agramunt-Puig, C. Navau, A. Sanchez, J. Sort, and J. Nogués, "Tunable high-field magnetization in strongly exchange-coupled

freestanding Co/CoO core/shell coaxial nanowires," ACS Appl. Mater. Interfaces **8**, 22477–22483 (2016).
[9]A. Sharma, J. Tripathi, S. Tripathi, Y. Kumar, K. C. Ugochukwu, D. Kumar, M. Gupta, and R. J. Chaudhary, "Exchange bias in Co/CoO thin films deposited onto self-assembled nanosphere arrays," J. Magn. Magn. Mater. **510**, 166599 (2020).
[10]P. Miltényi, M. Gierlings, J. Keller, B. Beschoten, G. Güntherodt, U. Nowak, and K. D. Usadel, "Diluted antiferromagnets in exchange bias: Proof of the domain state model," Phys. Rev. Lett. **84**, 4224–4227 (2000).
[11]B. Beschoten, J. Keller, P. Miltényi, and G. Güntherodt, "Domain state model for exchange bias: Thickness dependence of diluted antiferromagnetic $Co_{1-y}O$ on exchange bias in Co/CoO," J. Magn. Magn. Mater. **240**, 248–250 (2002).
[12]Z. Hussain and V. R. Reddy, "Role of anti-ferromagnetic layer thickness in exchange bias: Case study of Co/CoO with Kerr microscopy," Mater. Res. Express **6**, 066109 (2019).
[13]Z. Hussain and V. Raghavendra Reddy, "Kerr microscopy study of thermal and athermal training effects in a Co/CoO exchange bias system," J. Appl. Phys. **122**, 103903 (2017).
[14]I. N. Krivorotov, H. W. Yan, E. Dan Dahlberg, and A. Stein, "Exchange bias in macroporous Co/CoO," J. Magn. Magn. Mater. **226–230**, 1800–1802 (2001).
[15]D. Kumar, S. Singh, and A. Gupta, "Effect of interface roughness on exchange coupling in polycrystalline Co/CoO bilayer structure: An *in situ* investigation," J. Appl. Phys. **120**, 085307 (2016).
[16]A. N. Dobrynin, P. Warin, A. Vorobiev, and D. Givord, "On the origin of positive exchange bias and coercivity enhancement in proximity to the blocking temperature," J. Magn. Magn. Mater. **520**, 166707 (2021).
[17]V. L. Kurichenko, D. Y. Karpenkov, and A. Y. Degtyarenko, "Experimental and micromagnetic investigation of texture influence on magnetic properties of anisotropic Co/Co_3O_4 exchange-bias composites," J. Magn. Magn. Mater. **565**, 170232 (2023).
[18]S. Goswami, P. Gupta, S. Nayak, S. Bedanta, Ò. Iglesias, M. Chakraborty, and D. De, "Dependence of exchange bias on interparticle interactions in Co/CoO core/shell nanostructures," Nanomaterials **12**, 3159 (2022).
[19]M. Ghoshani, M. Mozaafari, P. S. Normile, J. A. de Toro, and A. Al-Nabhani, "Core size and interface impact on the exchange bias of cobalt/cobalt oxide nanostructures," Magnetochemistry **7**, 40 (2021).
[20]H. Ahmadvand, S. R. Safdari, A. Nozad Golikand, P. Dasgupta, A. Poddar, and H. Salamati, "Exchange bias in $Co/CoO/Co_3O_4$ nanostructures," J. Magn. Magn. Mater. **377**, 19–23 (2015).
[21]B. You, Y. X. Wang, Y. L. Zhao, L. Sun, W. Sheng, M. H. Pan, J. Du, A. Hu, and M. Lu, "Exchange bias in Co/Co_3O_4 bilayers," J. Appl. Phys. **93**, 6587–6589 (2003).
[22]Y. X. Wang, Y. J. Zhang, Y. M. Cao, M. Lu, and J. H. Yang, "Properties of exchange biased Co/Co_3O_4 bilayer films," J. Alloys Compd. **450**, 128–130 (2008).
[23]L. Qiao, H. Y. Xiao, H. M. Meyer, J. N. Sun, C. M. Rouleau, A. A. Puretzky, D. B. Geohegan, I. N. Ivanov, M. Yoon, W. J. Weber, and M. D. Biegalski, "Nature of the band gap and origin of the electro-/photo-activity of Co_3O_4," J. Mater. Chem. C **1**(31), 4628–4633 (2013).
[24]T. Blachowicz and A. Ehrmann, "Exchange bias in thin films—An update," Coatings **11**, 122 (2021).
[25]A. Tillmanns, S. Oertker, B. Beschoten, G. Güntherodt, C. Leighton, I. K. Schuller, J. Nogués, and J. Nogués, "Magneto-optical study of magnetization reversal asymmetry in exchange bias," Appl. Phys. Lett. **89**, 202512 (2006).
[26]D. Herrmann-Ronzaud, P. Burlet, and J. Rossat-Mignod, "Equivalent type-II magnetic structures: CoO, a collinear antiferromagnet," J. Phys. C: Solid State Phys. **11**, 2123 (1978).
[27]D. Tripathy and A. O. Adeyeye, "Perpendicular anisotropy and out-of-plane exchange bias in nanoscale antidot arrays," New J. Phys. **13**, 023035 (2011).
[28]A. Sharma, S. Tripathi, and K. C. Ugochukwu, "Exchange bias in nanosize Co/CoO triangles," J. Magn. Magn. Mater. **326**, 97–102 (2013).
[29]S. Maat, K. Takano, S. S. P. Parkin, and E. E. Fullerton, "Perpendicular exchange bias of Co/Pt multilayers," Phys. Rev. Lett. **87**, 087202 (2001).
[30]M. Salaheldeen, A. Nafady, A. M. Abu-Dief, R. Díaz Crespo, M. P. Fernández-García, J. P. Andrés *et al.*, "Enhancement of exchange bias and perpendicular magnetic anisotropy in CoO/Co multilayer thin films by tuning the alumina template nanohole size," Nanomaterials **12**, 2544 (2022).
[31]E. Menéndez, T. Dias, J. Geshev, J. F. Lopez-Barbera, J. Nogués, R. Steitz, B. J. Kirby, J. A. Borchers, L. M. C. Pereira, A. Vantomme, and K. Temst, "Interdependence between training and magnetization reversal in granular Co–CoO exchange bias systems," Phys. Rev. B **89**, 144407 (2014).
[32]E. Menéndez, L. E. S. Silva, G. Johann, J. Sort, and T. Dias, "Unraveling the origin of training in granular Co–CoO exchange bias systems with buried antiferromagnetic constituents," J. Magn. Magn. Mater. **478**, 170–174 (2019).
[33]R. Wu, J. Z. Wei, X. L. Peng, J. B. Fu, S. Q. Liu, Y. Zhang, Y. H. Xia, C. S. Wang, Y. C. Yang, and J. B. Yang, "The asymmetric magnetization reversal in exchange biased granular Co/CoO films," Appl. Phys. Lett. **104**, 182403 (2014).
[34]J. G. Ovejero, V. Godinho, B. Lacroix, M. A. García, A. Hernando, and A. Fernández, "Exchange bias and two steps magnetization reversal in porous Co/CoO layer," Mater. Des. **171**, 107691 (2019).
[35]U. Nowak, K. D. Usadel, J. Keller, P. Miltényi, B. Beschoten, and G. Güntherodt, "Domain state model for exchange bias. I. Theory," Phys. Rev. B **66**, 014430 (2002).
[36]S. Brems, K. Temst, and C. Van Haesendonck, "Origin of the training effect and asymmetry of the magnetization in polycrystalline exchange bias systems," Phys. Rev. Lett. **99**, 067201 (2007).
[37]J. De Clercq, A. Vansteenkiste, M. Abes, K. Temst, and B. van Waeyenberge, "Modelling exchange bias with MuMax^3," J. Phys. D: Appl. Phys. **49**, 435001 (2016).
[38]G. Panchal, R. J. Choudhary, M. Kumar, and D. M. Phase, "Interfacial spin glass mediated spontaneous exchange bias effect in self-assembled $La_{0.7}Sr_{0.3}MnO_3$:NiO nanocomposite thin films," J. Alloys Compd. **796**, 196–202 (2019).
[39]F. Radu, M. Etzkorn, T. Schmitte, R. Siebrecht, A. Schreyer, K. Westerholt, and H. Zabel, "Asymmetric magnetization reversal on exchange biased CoO/Co bilayers," J. Magn. Magn. Mater. **240**, 251–253 (2002).
[40]S. R. Ali, M. R. Ghadimi, M. Fecioru-Morariu, B. Beschoten, and G. Güntherodt, "Training effect of the exchange bias in Co/CoO bilayers originates from the irreversible thermoremanent magnetization of the magnetically diluted antiferromagnet," Phys. Rev. B **85**, 012404 (2012).
[41]E. Popova, H. Loosvelt, M. Gierlings, L. H. A. Leunissen, R. Jonckheere, C. van Haesendonck, and K. Temst, "Magnetization reversal in exchange biased Co/CoO patterns," Eur. Phys. J. B **44**, 491–500 (2005).
[42]F. Radu, M. Etzkorn, R. Siebrecht, T. Schmitte, K. Westerholt, and H. Zabel, "Interfacial domain formation during magnetization reversal in exchange-biased CoO/Co bilayers," Phys. Rev. B **67**, 134409 (2003).
[43]B. Kaeswurm and K. O'Grady, "The origin of athermal training in polycrystalline metallic exchange bias thin films," Appl. Phys. Lett. **99**, 222508 (2011).
[44]A. G. Biternas, R. W. Chantrell, and U. Nowak, "Dependence of training effect on the antiferromagnetic structure of exchange-bias bilayers within the domain-state model," Phys. Rev. B **89**, 184405 (2014).
[45]C. Binek, "Training of the exchange-bias effect: A simple analytic approach," Phys. Rev. B **70**, 014421 (2004).
[46]C. Binek, X. He, and S. Polisetty, "Temperature dependence of the training effect in a Co/CoO exchange-bias layer," Phys. Rev. B **72**, 054408 (2005).